atmosphere

MDPI

Communication

Study of Relative Humidity Vertical Distribution Characteristics before Precipitation by Microwave Radiometer Data over Southeast China

Yongjiang Yu [1,2,*], Yan Zou [3] and Weihua Pan [1,2]

[1] Fujian Key Laboratory of Severe Weather, Fuzhou 350007, China
[2] Fujian Institute of Meteorological Science, Fuzhou 350007, China
[3] Fujian Climate Centre, Fuzhou 350007, China
* Correspondence: fjqxyyj@163.com

Abstract: We investigated the relative humidity (RH) vertical distribution characteristics before precipitation using microwave radiometer measurements over southeast China in 2021. The superposed epoch method is used to analyze the profile and vertical statistical characteristics and evolution of RH during precipitation events. There is a shallow, high-humidity area on the ground, with a thickness of about 0.1–0.2 Km, from 12 to 8 h before precipitation. An obvious dry layer appears in the lower layer near the ground 8–0 h before precipitation, with a thickness of about 1 km and humidity of less than 80%, which continues until the appearance of precipitation. The water vapor content in the air begins to accumulate and the humidity increases before the occurrence of LRs, MRs, and HRs, classified by total rainfall. The SDPs, MDPs, and LDPs, which are classified by precipitation duration, showed more obvious and significant characteristics of humidity increase. The statistical analysis of the 44 precipitation cases shows that the relative humidity on the ground and in the air increases significantly before precipitation, and the vertical distribution of the relative humidity and the increase in the water vapor content in the air have a more direct and obvious impact on the precipitation duration. The deep and high-humidity area of 2–4 km is conducive to maintaining the precipitation process for a long time.

Keywords: relative humidity; microwave radiometer data; total rainfall; precipitation duration; vertical distribution

Citation: Yu, Y.; Zou, Y.; Pan, W. Study of Relative Humidity Vertical Distribution Characteristics before Precipitation by Microwave Radiometer Data over Southeast China. *Atmosphere* **2023**, *14*, 513. https://doi.org/10.3390/atmos14030513

Academic Editors: Duanyang Liu, Hongbin Wang and Shoupeng Zhu

Received: 5 February 2023
Revised: 26 February 2023
Accepted: 1 March 2023
Published: 7 March 2023

1. Introduction

Moisture plays an important role in many weather processes, especially in continuous precipitation process. The root cause of abnormally heavy precipitation is closely related to the water vapor supply and transportation under the background of large-scale circulation [1,2]. Atmospheric water vapor content and vertical distribution are crucial meteorological parameters for understanding atmospheric thermodynamic processes [3]. On the one hand, the water vapor content directly influences the global hydrological cycle, which is closely related to atmospheric energy transmission, radiation budget balance, cloud and rain formation, and climate change [4–6]. On the other hand, the microphysical features of precipitation, which can be reflected by its vertical structure, are helpful in understanding the thermodynamic and dynamic properties of precipitation systems.

The influence of water vapor at different heights on surface precipitation is different [7,8]. The sensitivity of the structure and strength of a squall line in the initial and early development stages to initial low-level humidity and environment vertical wind shear are investigated in a two-dimensional idealized squall line simulation using the WRF model. The results of the sensitivity test of low-level humidity indicate that increasing low-level humidity is favorable for convective triggering and stronger convective systems [9]. The radar reflectivity and precipitation rate from the Precipitation Radar onboard

Tropical Rainfall Measuring Mission satellite are obtained over the global tropical regions (35° S–35° N) during the period from 2007 to 2012, combined with coincident vertical velocity at 400 hPa, relative humidity at 850 hPa, and lower tropospheric stability from European Centre for Medium-Range Weather Forecasts reanalysis. The results imply that coincident vertical velocity at 400 hPa and relative humidity at 850 hPa are most likely to play a dominant role in dictating the vertical development of convection [10]. The analysis of cyclone heavy rain processes with different low-level humidity conditions in Qingdao indicated that the relative humidity at 850 hPa before the heavy rain was higher and the duration of rainfall was longer [11].

The traditional method of detecting atmospheric water vapor and temperature profiles is based on the radiosonde (RS) carried by a sounding balloon. It has the advantages of high accuracy and reliability, low power consumption, light weight, and small size. However, it is influenced by limits of equipment and manpower costs, the launch frequency of RS is relatively low [3]. Additionally, the motion path of the sounding balloon can vary, largely due to the horizontal advection and variable ascent rate [12], which will cause measured drift in the atmospheric profile. The microwave radiometer (MWR) is a passive remote sensing instrument that provides vertical profiles of atmospheric temperature and water vapor content by measuring the thermal radiation emitted by the atmosphere. Compared with the RS, it has applicability due to the advantages of high temporal resolution, reasonable vertical resolution, and ability to automatically measure under almost all-weather conditions [13–15]. In addition, the MWR can also provide other atmospheric parameters, such as cloud base height, integrated water vapor (IWV), and liquid water path (LWP), which are important for evaluating cloud water resources, climate change, and precipitation [16–18]. Performance of MWR was also estimated by comparing with the RS data. The temperature profile measured by the microwave radiometer was better under cloudy conditions, while the RH profile had higher accuracy under cloud-free conditions [19–21]. The comparison of temperature and vapor density obtained from MWR and RS observations during the Integrative Monsoon Frontal Rainfall Experiment Show that: for all sky conditions, the temperature of MWR has a good agreement with that of RS. The vapor density from two measurements also shows reasonable agreement [22–24].

In the past, research on microwave radiometer retrieval data mainly focused on the evolution characteristics of the total accumulated water vapor and cloud liquid water in the whole layer before the beginning of precipitation. There are few studies on the distribution and evolution characteristics of the vertical profile of water vapor and relative humidity, and the analysis of the contribution of moisture to precipitation duration is also less involved.

Jian'ou city is located to the south of Wuyi Mountains. Subtropical monsoon climate prevailing at this city brings significant seasonal differences in temperature and rainfall. Jian'ou has abundant rainfall, with an average annual precipitation of 1753.7 mm, and the disasters caused by precipitation in this city are very serious. In this study, Jian'ou is adopted as a representative city for the southeast China to investigate the vertical structure characteristics of humidity in different rainfall regimes using continuous MWR observations in 2021.

The remainder of this paper is organized as follows. Section 2 introduces the dataset and method used in this study. Our analyses of RH variation and its vertical distribution before precipitation are presented and discussed in Section 3, and conclusions are given in Section 4.

2. Materials and Methods

The observation station selected in this study is located at Jian'ou National Reference Climate Station (118°19′23″ E, 27°03′10″ N, UTC +8, 150 m above sea level) in southeast China from Jan to Dec 2021 to explore the humidity properties of the atmosphere before different rainfall regimes (Figure 1).

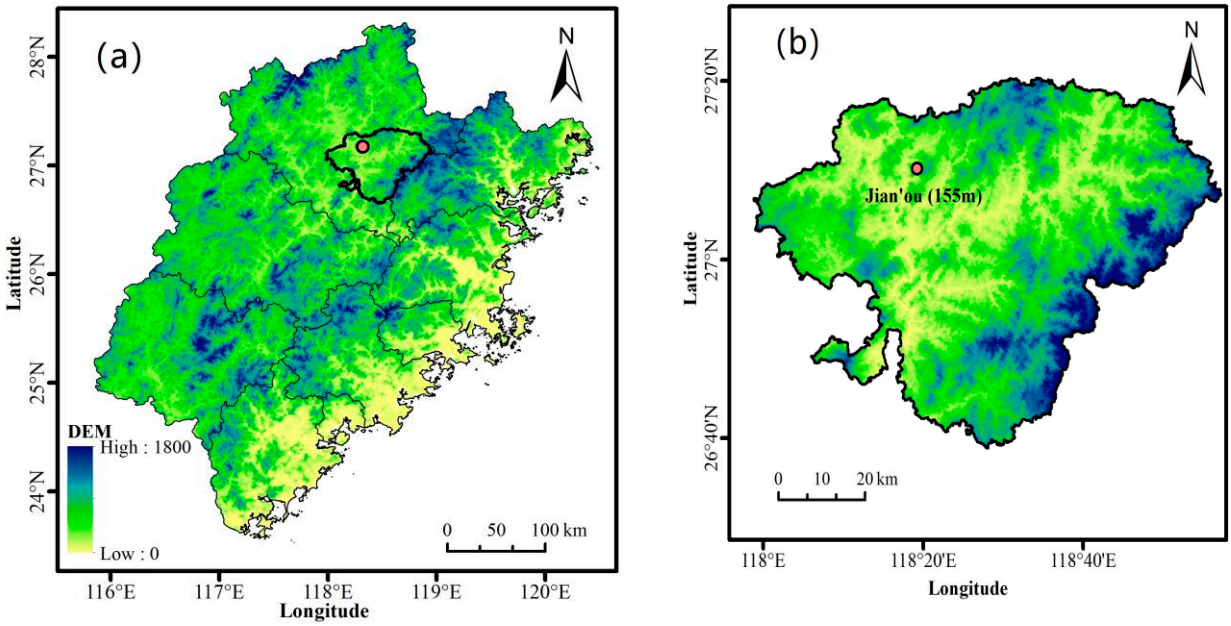

Figure 1. Geographical map of study area ((**a**) is Fujian Province, (**b**) is Jian'ou Station).

2.1. Instruments

The MWR is a QFW6000 unit independently manufactured by China Research Institute of Radiowave Propagation. It observes brightness temperature in 48 channels, including 24 K bands (22–32 GHz) and 24 V bands (51–59 GHz). Combined with ambient temperature, pressure, and relative humidity from the meteorological sensors attached to MWR, atmospheric profiles (temperature, vapor density, and relative humidity) are retrieved from these brightness temperatures. Atmospheric profiles derived from MWR have a temporal resolution of ∼3 min and vertical resolutions of 50 m from the surface to 0.5 km, 100 m from 0.5 to 2.0 km, and 250 m from 2.0 to 10.0 km.

RS is usually used as a standard criterion to evaluate other measurements because it detects atmospheric parameters directly with various correction methods for improving its accuracy. Atmospheric temperature, water vapor density, and relative humidity profiles retrieved from the MWR were verified using radiosonde soundings.

Comparison of temperature and relative humidity obtained from MWR and RS were operated at Fu'zhou station during December 2016, which have the same climate with Jian'ou in the north of Fujian Province. For all sky conditions, the temperature of MWR has good agreement with that of RS and a correlation coefficient (R) of 0.995, with a root mean square error of 0.3–0.22 °C. The relative humidity from two measurements also shows reasonable agreement, with an R of 0.743 and a root mean square error of 2.5–12.55%. The relative humidity data obtained from MWR at Jian'ou station was filtered strictly by removing missing data and singular value number during 2021. So, the atmospheric profiles data used in this paper were successive, stable, and credible.

2.2. Data and Methods

The MWR dataset has the temporal resolution of 3 min. Since the time step of the data is not an integer, in order to facilitate the analysis and maintain the data accuracy as much as possible, before the individual statistics, this paper takes the average value of the physical quantity in a total of 5 min before and after a certain time as the physical quantity value at that time, and it is reasonable to set the temporal resolution as 5 min.

Therefore, select and classify rainfall samples according to the following criteria:

1. Investigate the hourly precipitation data of Jian'ou Station from 1 January to 31 December 2021, and continuous precipitation as a sample.

2. Eliminate the case in which precipitation occurred in the 12 h period before the start of precipitation, and eliminate the impact of early precipitation on the inversion data of ground-based microwave radiometer.
3. Eliminate the weak rainfall samples with 1 mm rainfall in the first hour and less than 6 h duration.
4. The rainfall samples are divided into light rain (LR, cumulative rainfall is 0–5 mm), moderate rain (MR, cumulative rainfall is 5–10 mm), and heavy rain (HR, cumulative rainfall > 10 mm) according to the cumulative rainfall.
5. The rainfall samples are divided into short-duration precipitation (SDP, precipitation duration is 1–3 h), medium-duration precipitation (MDP, precipitation duration is 4–8 h), and long-duration precipitation (LDP, precipitation duration is >9 h) according to the duration of rainfall.

The occurrence time of precipitation is set as the 0-hour time, and the 1 h before precipitation is set as −1 h while the 1 h after precipitation is set as +1 h. If no precipitation occurs during the 12 h before 0-hour time, and the accumulated precipitation within 1 h after 0 time is more than 1 mm or the precipitation duration is greater than 6 h, then the case is picked. Using this principle, 44 samples were selected to investigate the temporal variation in relative humidity (see Table 1). According to the total rainfall, there are 12 LRs, 13 MRs, and 19 HRs. According to the precipitation duration, there are 23 SDPs, 13 MDPs, and 8 LDPs.

Table 1. Cases information of precipitation at Jian'ou station during 2021.

No.	Start Time of Precipitation	Precipitation Duration/h	Cumulative Rainfall/mm	Classification by Duration	Classification by Total Rainfall
1	2021/2/16 18:00	6	4.8	MDP	LR
2	2021/3/1 23:00	5	7.3	MDP	MR
3	2021/3/4 23:00	2	2.9	SDP	LR
4	2021/3/11 5:00	6	8.3	MDP	MR
5	2021/3/30 18:00	1	10.0	SDP	HR
6	2021/4/22 13:00	1	4.5	SDP	LR
7	2021/4/24 20:00	13	19.1	LDP	HR
8	2021/4/27 8:00	4	2.5	MDP	LR
9	2021/5/4 16:00	3	7.9	SDP	MR
10	2021/5/7 17:00	11	27.0	LDP	HR
11	2021/5/13 18:00	1	8.1	SDP	MR

Table 1. *Cont.*

No.	Start Time of Precipitation	Precipitation Duration/h	Cumulative Rainfall/mm	Classification by Duration	Classification by Total Rainfall
12	2021/5/16 17:00	1	5.3	SDP	MR
13	2021/5/23 19:00	4	8.8	MDP	MR
14	2021/5/27 5:00	8	15.3	MDP	HR
15	2021/5/31 16:00	8	8.2	MDP	MR
16	2021/6/4 0:00	5	10.6	MDP	HR
17	2021/6/19 14:00	2	2.9	SDP	LR
18	2021/6/21 16:00	7	23.8	MDP	HR
19	2021/6/28 2:00	16	56.9	LDP	HR
20	2021/6/29 16:00	2	21.8	SDP	HR
21	2021/7/20 15:00	1	6.1	SDP	MR
22	2021/7/23 15:00	2	7.0	SDP	MR
23	2021/7/24 14:00	2	3.4	SDP	LR
24	2021/7/27 20:00	2	26.5	SDP	HR
25	2021/7/28 16:00	3	36.0	SDP	HR
26	2021/7/31 0:00	1	1.0	SDP	LR
27	2021/7/31 20:00	3	55.9	SDP	HR
28	2021/8/1 17:00	9	35.6	LDP	HR
29	2021/8/2 16:00	1	9.4	SDP	MR
30	2021/8/3 15:00	3	16.0	SDP	HR
31	2021/8/11 18:00	1	5.5	SDP	MR
32	2021/8/14 16:00	2	3.1	SDP	LR
33	2021/8/15 17:00	5	27.8	MDP	HR

Table 1. *Cont.*

No.	Start Time of Precipitation	Precipitation Duration/h	Cumulative Rainfall/mm	Classification by Duration	Classification by Total Rainfall
34	2021/8/20 16:00	3	12.0	SDP	HR
35	2021/8/28 18:00	1	1.2	SDP	LR
36	2021/9/8 20:00	3	10.5	SDP	HR
37	2021/9/12 16:00	1	3.6	SDP	LR
38	2021/10/19 18:00	16	12.1	LDP	HR
39	2021/11/2 4:00	6	6.4	MDP	MR
40	2021/11/13 1:00	6	1.9	MDP	LR
41	2021/11/21 19:00	14	17.9	LDP	HR
42	2021/12/16 5:00	8	5.8	MDP	MR
43	2021/12/20 20:00	21	15.7	LDP	HR
44	2021/12/25 12:00	13	3.2	LDP	LR

In order to study the change characteristics of relative humidity and its vertical structure before the beginning of different types of precipitation, temporal variations in the relative humidity were analyzed with superposed epoch method, which highlights the effect of the factor in the key time periods while weakening the effects of other factors [25].

The superposed epoch is a row–column array in which the "response" index values filling any row are data pertaining to a single key event. Thus, the number of rows is the sample size of such events. The columns line up the index values in fixed time relation to the key times; column averages comprise the "superposed epoch analysis." By this averaging method, any fluctuations in the response index that are locked in time relative to the key time column are preserved in the average, whereas fluctuations shifting in time from row to row are averaged out [26].

3. Results and Discussion

Because the RH can provide information about hydrometeors in the atmosphere, it is a key parameter used in numerical models and precipitation forecast. We analyzed the variation in the RH before and after precipitation using the superposed epoch method. This section first presents statistical characteristics of RH from MWR before precipitation. Moreover, retrieval applications of MWR in rainy environments are further studied to support nowcasting and precipitation duration estimation.

3.1. Variation in RH before and after Precipitation Classify by Total Rainfall

Figure 2 shows statistical characteristics of relative humidity from 12 precipitation cases of LR. The relative humidity on the ground and in the air began to increase 12–6 h before the start of precipitation, and the relative humidity increased in the near ground layer (below 0.2 km) and the middle and low layer (1–3 km), but the humidity of these two

layers did not reach saturation (exceeded 80%). There is an obvious dry layer (humidity is lower than 70%) between the two layers of accumulated water vapor growth, and the thickness of the dry layer is about 0.8 km; 6–0 h before the start of precipitation, the wet layer near the ground began to rise, and a dry layer with a thickness of 1 km appeared near the ground until the occurrence of precipitation. The humidity continues to increase between 1–3 km during −6 to 0 h, forming a high-humidity area.

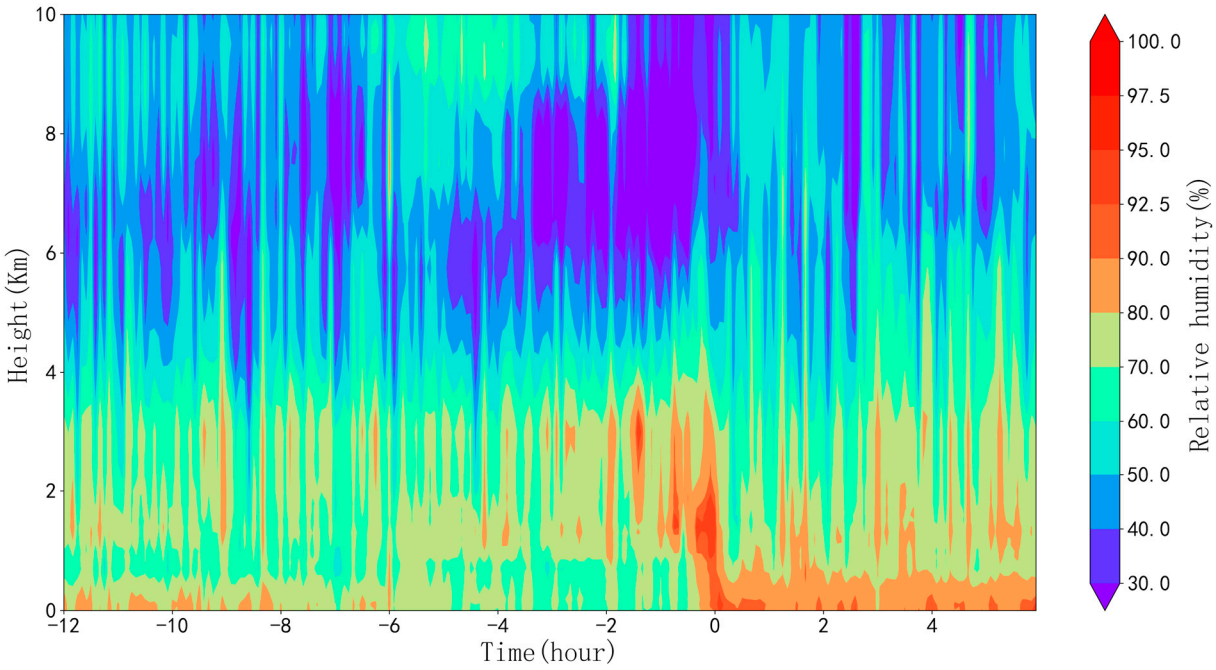

Figure 2. Vertical distributions of relative humidity during 12 h before and 6 h after the start of LRs in 2021.

The statistical analysis results of 13 precipitation cases of MR are shown in Figure 3. It can be seen that the ground and air humidity increased 12–8 h before the precipitation, especially the water vapor content near the ground increased significantly, the thickness of the high-humidity area on the ground reached 0.2 km, and the relative humidity exceeded 90%. After −8 h, the humidity in the lower layer decreased, an obvious dry layer appeared below 2 km, and the water vapor began to accumulate in the high humidity area around 3 km in the middle layer, and the wet layer thickened and became nearly saturated, until the appearance of precipitation.

Figure 4 illustrates the vertical distributions of relative humidity during 12 h before and 6 h after the start of 19 HR cases. From 12 to 8 h before the beginning of precipitation, there is a process of significant humidity increase on the ground, with humidity exceeding 80% and thickness only about 0.1 km, and then the humidity near the ground decreases, and a dry layer with humidity less than 70% appears below 1 km. From 12 h before the precipitation, the process of external water vapor transport and humidity increase in the middle and lower layers (1–4 km) began to occur, and the wet layer was thick.

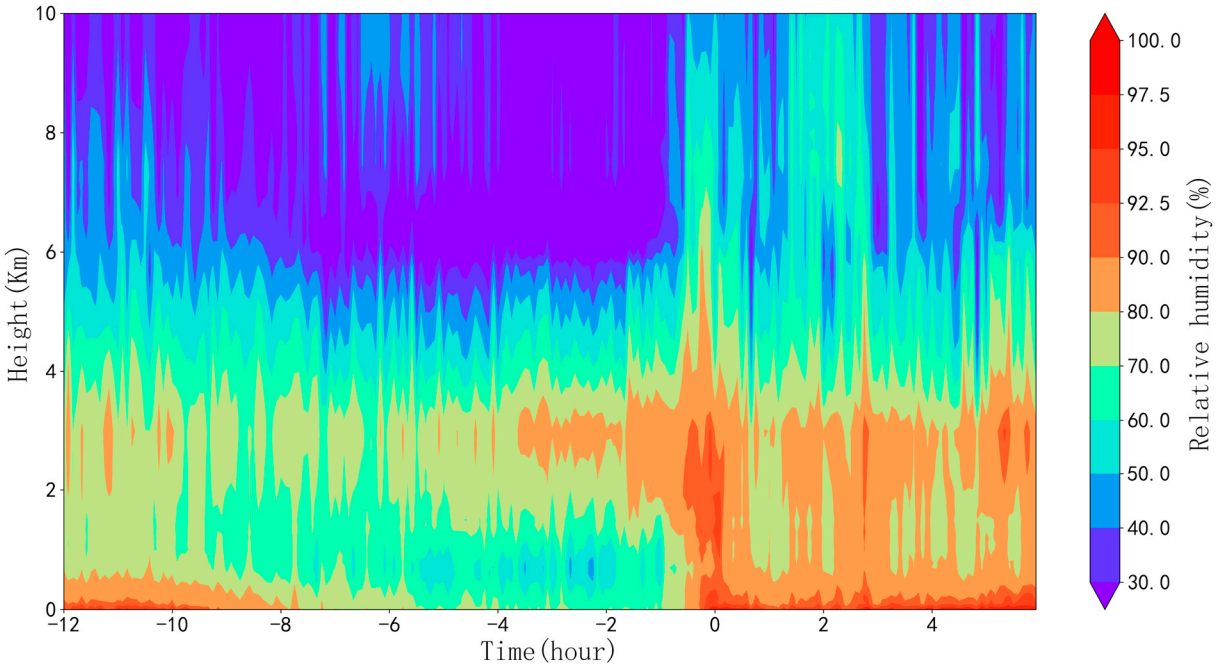

Figure 3. Vertical distributions of relative humidity during 12 h before and 6 h after the start of MRs in 2021.

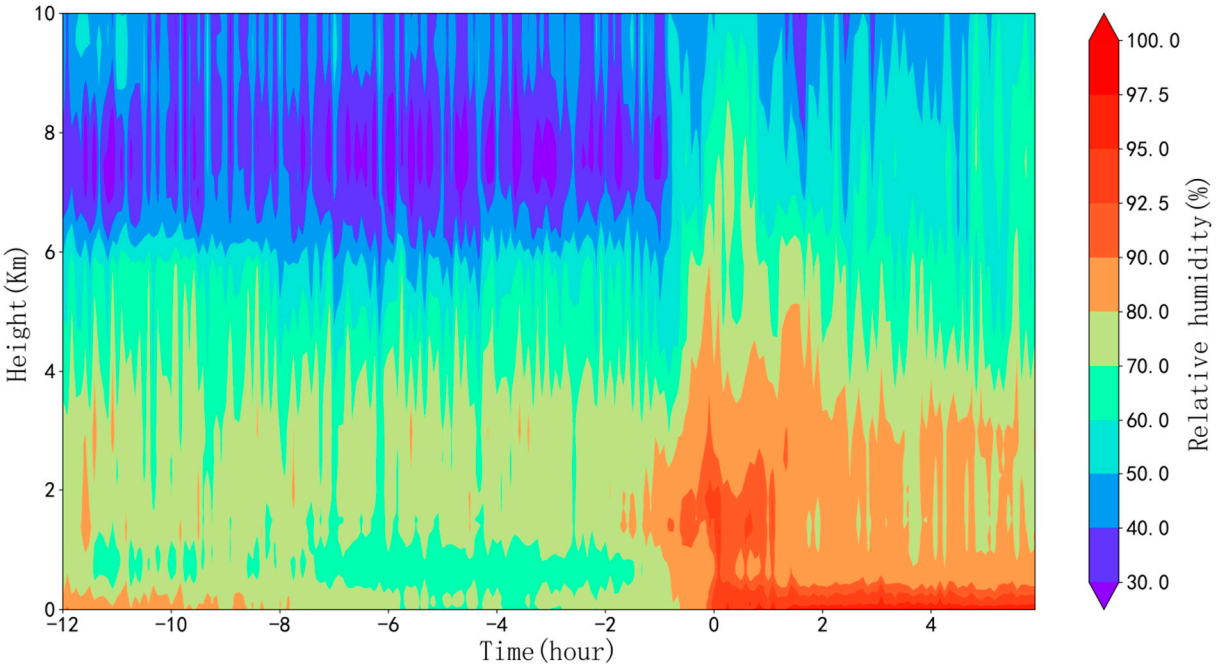

Figure 4. Vertical distributions of relative humidity during 12 h before and 6 h after the start of HRs in 2021.

3.2. Variation in RH before and after Precipitation Classify by Duration

Precipitation is when water vapor in the atmosphere condenses and becomes heavy enough to fall to the ground. Clouds are made of water vapor under different conditions, including variations in relative humidity and air pressure, the vapor particles can begin to combine and form much larger droplets. The increase in relative humidity, which in turn leads to the accumulation of water vapor, is a necessary condition for the formation of

precipitation. It not only affects the total rainfall in the rainfall regimes, but also helps to maintain the rainfall regimes for a long time.

Figure 5 presents the mean RH profile from 0 to 10 km during 12 h before and 6 h after the occurrence of 23 SDP cases at Jian'ou station. It is shown that the ground relative humidity began to increase significantly 12–8 h before the start of precipitation, and average relative humidity exceeds 80%, but the high humidity area near the ground is shallow, about 0.2 km thick. From −8 to 0 h before the beginning of precipitation, with the increase in water vapor, the relative humidity on the ground decreases, and a dry layer appears near the ground. From −4 to 0 h before the precipitation, the water vapor in the air began to increase gradually, and the humidity layer at the height of 1–4 km began to thicken. Within 2 h before the precipitation, the humidity increased rapidly and approached saturation, with the average humidity layer thickness reaching 3 km.

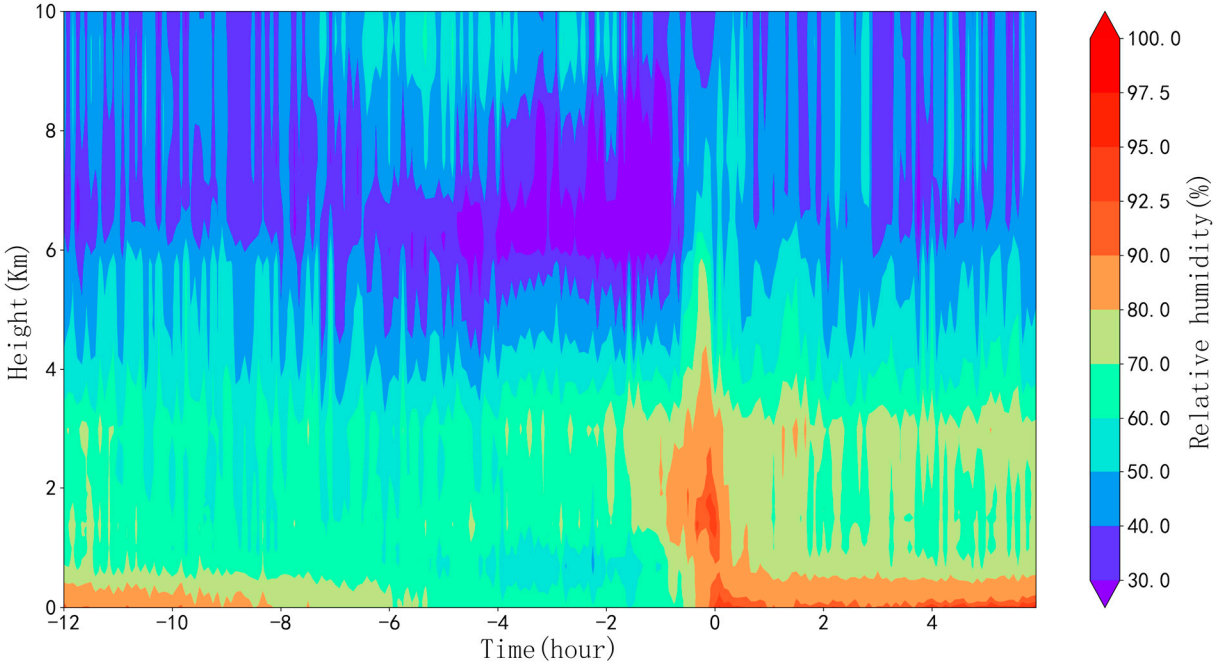

Figure 5. Vertical distributions of relative humidity during 12 h before and 6 h after the start of SDPs in 2021.

The temporally averaged RH profiles during 12 h before and 6 h after the occurrence time of the 13 MDP events are presented in Figure 6. It is shown that the ground relative humidity began to increase significantly 12 h before the beginning of precipitation, and a shallow and discontinuous high humidity layer appeared, with the average relative humidity reaching more than 80%. Continuous and deep wet areas appear, with average humidity of more than 80% and average thickness of 2.2 Km, between 1.8–4 Km in the air. There is an obvious dry layer between the high humidity layer on the ground and in the air, with a thickness of about 1.5 km. With the further transportation of water vapor within 2 h before the precipitation, the dry layer between the ground and the air disappears, the thickness of the humidity layer reaches 5–6 Km, and the average humidity exceeds 90%, which is close to saturation.

Figure 7 presents the statistical characteristics of the relative humidity profile during the 8 LDP cases at Jian'ou station before precipitation. It can be seen that 12–8 h before the start of precipitation, along with the water vapor transport, a deep moisture layer begins to appear in the middle and low layers, with a thickness of 5–6 Km and an average humidity of more than 80%; the layer between 2 and 4 km is the water vapor concentration zone, which air close to saturation and humidity is more than 90%. From −8 to −1 h before precipitation, the bottom atmospheric humidity began to decrease. The atmospheric

moisture content is low within 1 km above the ground, and the humidity is less than 80%. The moisture is mainly concentrated in the middle and upper layers of 1.5–5.5 km, the relative humidity is more than 80%, and the local humidity exceeds 90%.

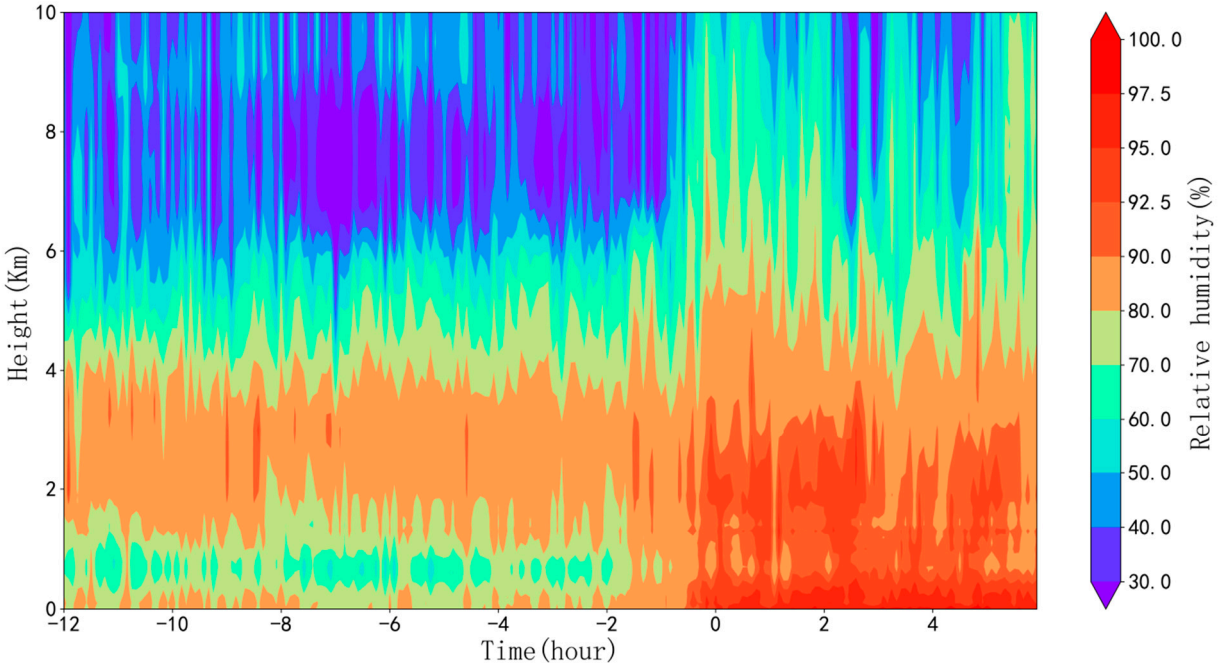

Figure 6. Vertical distributions of relative humidity during 12 h before and 6 h after the start of MDPs in 2021.

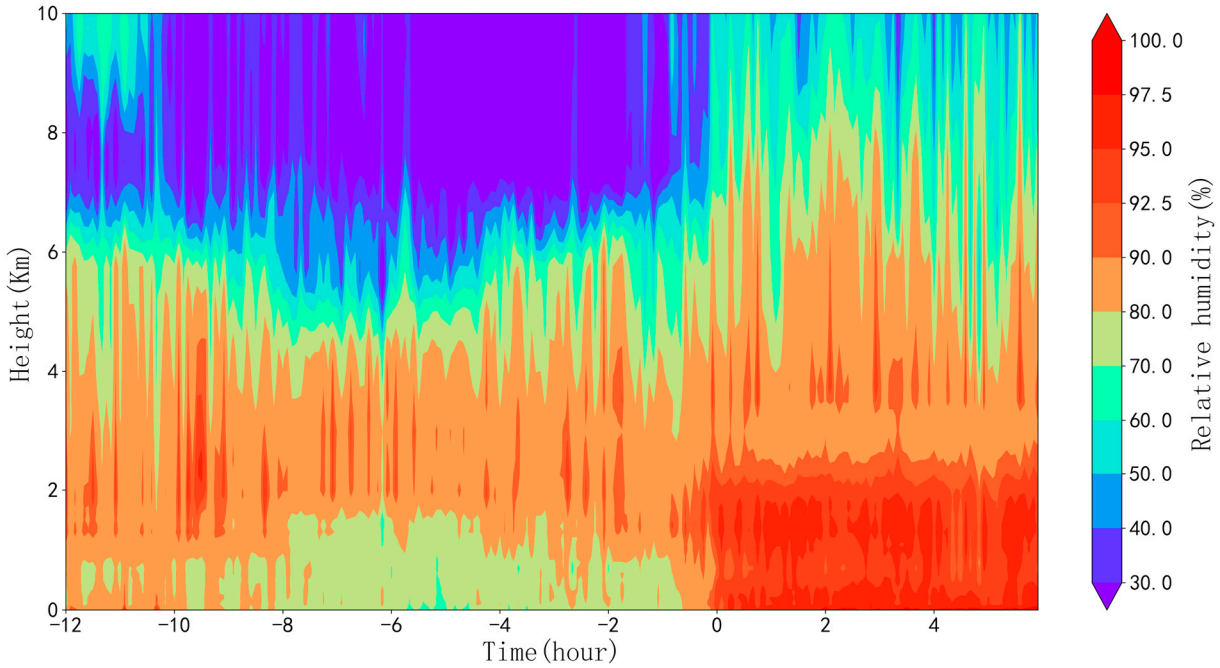

Figure 7. Vertical distributions of relative humidity during 12 h before and 6 h after the start of LDPs in 2021.

4. Summary and Conclusions

The main objective of this study was to investigate the variation and vertical distributions of RH before precipitation. We used the superposed epoch method to analyze the profile of RH during precipitation events.

There is a shallow high humidity area on the ground, with a thickness of about 0.1–0.2 km, from 12 to 8 h before precipitation. An obvious dry layer appears in the lower layer near the ground 8–0 h before precipitation, with a thickness of about 1 km and humidity of less than 80%, which continues until the appearance of precipitation.

The water vapor content in the air began to accumulate and the humidity increased before the occurrence of LRs, MRs, and HRs, which is classified by total rainfall. The increase in air humidity continues from 12 h before precipitation to the beginning of precipitation. The wet layer thickness of LRs is the thinnest, and the height of wet layer is also low. Before precipitation of MRs and HRs, the characteristics of water vapor accumulation in the atmosphere are similar. High humidity areas with relative humidity greater than 80% are continuous and deep. Before the start of HRs, the thickness of the humidity layer (RH > 80%) can reach 4 km and the height can reach 6 km.

The SDPs, MDPs, and LDPs, which are classified by precipitation duration, also showed statistical characteristics of significant increase in humidity. There is a high humidity area in the middle and low layers until 2 h before SDPs. The 12–0 h before the occurrence of MDPs, a continuous and deep humidity layer appeared between 1.8 and 4 Km on the ground, with an average thickness of 2.2 Km. The humidity layer became thicker as the precipitation approached. The 12–6 h before LDPs, water vapor content below 6 km is very rich, and the thickness of high humidity area reaches 5–6 Km. After that, the humidity layer rises, and the high humidity layer between 1.5 and 5.5 km is maintained until the appearance of precipitation.

The statistical analysis of the filtered 44 precipitation cases shows that the relative humidity on the ground and in the air increases significantly before precipitation, and the vertical distribution of the relative humidity and the increase of the water vapor content in the air have a more direct and obvious impact on the precipitation duration. The deep and high humidity area of 2–4 km is conducive to maintaining the precipitation process for a long time.

A large number of numerical model simulations and reanalysis data analysis show that the physical quantities that affect the atmospheric thermal and dynamic environment during precipitation mainly include rising speed, relative humidity, temperature, and vertical wind shear. The transportation of warm and humid air leads to the increase in the convective available potential energy over the precipitation area. The increase in low-level humidity is favorable for convective triggering and stronger convective systems. The increased convective intensity and upward movement make it easier for new convective cells to form at the leading edge of the cold poll. The increased low-level humidity also leads to more precipitation, which raises the intensity of cold poor. Coincident vertical velocity at 400 hPa and relative humidity at 850 hPa most likely play a dominant role in dictating the vertical development of convection. The important causes of longer duration and the larger accumulated of precipitation was the higher relative humidity conditions and long-lasting upward motion, as well as continuous water vapor transport. Therefore, it is of great significance to strengthen the analysis of the of low-level jet and relative humidity vertical distribution by microwave radiometer data for the prediction of precipitation.

Author Contributions: Conceptualization, Y.Y.; Y.Z.; W.P.; methodology, Y.Y.; Y.Z.; software, Y.Y.; validation, Y.Z.; formal analysis, Y.Y.; Y.Z.; investigation, Y.Y.; Y.Z.; resources, Y.Y.; data curation, Y.Y.; writing—original draft preparation, Y.Y.; writing—review and editing, Y.Y.; visualization, W.P.; supervision, Y.Y.; project administration, Y.Y.; funding acquisition, Y.Y.; Y.Z. All authors have read and agreed to the published version of the manuscript.

Funding: This research was funded by the Open Research Fund of Fujian Provincial Meteorological Bureau (2021KX02), the National Key Research and Development Program of China (2019YFC1510303).

Institutional Review Board Statement: Not applicable.

Informed Consent Statement: Not applicable.

Data Availability Statement: The data were observed by Fujian Provincial Meteorological Bureau. If you want to obtain it, please apply through email (fjqxyyj@163.com).

Acknowledgments: The authors acknowledge the free use of the microwave radiometer data provided by Fujian Provincial Meteorological Bureau. We also appreciate the anonymous reviewers for their constructive comments and thoughtful suggestions.

Conflicts of Interest: The authors declare that they have no conflict of interest.

References

1. Zhang, L.; Du, L.; Chen, L. Analysis of Water Vapor Source and Transport Path of Abnormal Heavy Rain in Wuhan. *Meteorol. Environ. Sci.* **2014**, *37*, 69–74.
2. Wang, X.; Xu, G.; Yuan, K. Different characteristic analysis of inversion parameters for heavy rainfall and weak rainfall by microwave radiometer data. *Torrential Rain Disasters* **2016**, *35*, 227–233.
3. Jin, S.; Ma, Y.; Gong, W.; Liu, B.; Lei, L.; Fan, R. Characteristics of vertical atmosphere based on five-year microwave remote sensing data over Wuhan region. *Atmos. Res.* **2021**, *260*, 105710. [CrossRef]
4. Ramanathan, V.; Crutzen, P.J.; Kiehl, J.T.; Rosenfeld, D. Atmosphere—Aerosols, climate, and the hydrological cycle. *Science* **2001**, *294*, 2119–2124. [CrossRef] [PubMed]
5. Rosenfeld, D.; Lohmann, U.; Raga, G.B.; O'Dowd, C.D.; Kulmala, M.; Fuzzi, S.; Reissell, A.; Andreae, M.O. Flood or drought: How do aerosols affect precipitation? *Science* **2008**, *321*, 1309–1313. [CrossRef]
6. Obregon, M.A.; Costa, M.J.; Silva, A.M.; Serrano, A. Impact of aerosol and water vapour on SW radiation at the surface: Sensitivity study and applications. *Atmos. Res.* **2018**, *213*, 252–263. [CrossRef]
7. Qi, Y.; Fan, S.; Mao, J.; Li, B.; Guo, C.; Zhang, S. Impact of Assimilating Ground-Based Microwave Radiometer Data on the Precipitation Bifurcation Forecast: A Case Study in Beijing. *Atmosphere* **2021**, *12*, 551. [CrossRef]
8. Qi, Y.; Fan, S.; Li, B.; Mao, J.; Lin, D. Assimilation of Ground-Based Microwave Radiometer on Heavy Rainfall Forecast in Beijing. *Atmosphere* **2022**, *13*, 74. [CrossRef]
9. Gao, Y.; Sun, L.; Ma, X.; Meng, Z.; Cheng, K. The sensitivity of structure and strength of squall line to low-level humidity and environment vertical wind shear. *Trans. Atmos. Sci.* **2022**, *45*, 938–947. (In Chinese)
10. Liu, H.; Guo, J.; Chen, T.; Zhai, P. On the seasonal variation of various types of precipitation over global tropical ocean region: A perspective from TRMM measurements. *Chin. Sci. Bull.* **2017**, *62*, 90–104. (In Chinese) [CrossRef]
11. Liu, X.; Ma, Y.; Ling, Y.; Jiang, D.; Wan, F. Analysis of Two cyclone heavy rain processes with different low-level humidity conditions in Qingdao. *Meteorol. Sci. Technol.* **2019**, *47*, 818–829.
12. Bedoya-Velásquez, A.E.; Navas-Guzmán, F.; Moreira, G.D.A.; Román, R.; Cazorla, A.; Ortiz-Amezcua, P.; Benavent-Oltra, J.A.; Alados-Arboledas, L.; Olmo-Reyes, F.J.; Foyo-Moreno, I.; et al. Seasonal analysis of the atmosphere during five years by using microwave radiometry over a mid-latitude site. *Atmospheric Res.* **2019**, *218*, 78–89. [CrossRef]
13. Li, Q.; Wei, M.; Wang, Z.; Chu, Y. Evaluation and Improvement of the Quality of Ground-Based Microwave Radiometer Clear-Sky Data. *Atmosphere* **2021**, *12*, 435. [CrossRef]
14. Liu, M.; Liu, Y.-A.; Shu, J. Characteristics Analysis of the Multi-Channel Ground-Based Microwave Radiometer Observations during Various Weather Conditions. *Atmosphere* **2022**, *13*, 1556. [CrossRef]
15. Ma, R.; Li, X. Sounding Data from Ground-Based Microwave Radiometers for a Hailstorm Case: Analyzing Spatiotemporal Differences and Initializing an Idealized Model for Prediction. *Atmosphere* **2022**, *13*, 1535. [CrossRef]
16. Cui, C.; Wan, R.; Wang, B. The Mesoscale Heavy Rainfall Observing System (MHROS) over the middle region of the Yangtze River in China. *J. Geophys. Res. Atmos.* **2015**, *120*, 10399–10417. [CrossRef]
17. Huang, J.; Minnis, P.; Lin, B.; Yi, H.; Sun-Mack, S.; Fan, T.-F.; Ayers, J. Determination of ice water path in ice-over-water cloud systems using combined MODIS and AMSR-E measurements. *Geophys. Res. Lett.* **2006**, *33*. [CrossRef]
18. Lei, L.; Wang, Z.; Ma, Y.; Zhu, L.; Qin, J.; Chen, R.; Lu, J. Measurement of Solar Absolute Brightness Temperature Using a Ground-Based Multichannel Microwave Radiometer. *Remote Sens.* **2021**, *13*, 2968. [CrossRef]
19. Shi, Y.; Wei, J.; Qiao, Z.; Zhao, J.; Wang, G. Atmospheric Exploration of the Qinghai–Tibet Plateau during the East Asian Winter Monsoon (EAWM) from a Ground-Based Microwave Radiometer. *Atmosphere* **2022**, *13*, 549. [CrossRef]
20. Wei, J.; Shi, Y.; Ren, Y.; Li, Q.; Qiao, Z.; Cao, J.; Ayantobo, O.O.; Yin, J.; Wang, G. Application of Ground-Based Microwave Radiometer in Retrieving Meteorological Characteristics of Tibet Plateau. *Remote Sens.* **2021**, *13*, 2527. [CrossRef]
21. Xu, G.; Xi, B.; Zhang, W.; Cui, C.; Dong, X.; Liu, Y.; Yan, G. Comparison of atmospheric profiles between microwave radiometer retrievals and radiosonde soundings. *J. Geophys. Res. Atmos.* **2015**, *120*, 10313–10323. [CrossRef]
22. Xu, G.; Xi, B.; Zhang, W.; Cui, C.; Dong, X.; Liu, Y.; Yan, G. Cloud occurrence frequency and cloud liquid water path for non-precipitating clouds using ground-based measurements over central China. *J. Atmos. Sol.-Terr. Phys.* **2021**, *215*, 105575. [CrossRef]
23. Zhang, W.; Xu, G.; Liu, Y.; Yan, G.; Li, D.; Wang, S. Uncertainties of ground-based microwave radiometer retrievals in zenith and off-zenith observations under snow conditions. *Atmos. Meas. Tech.* **2017**, *10*, 155–165. [CrossRef]

24. Zhang, W.; Xu, G.; Xi, B.; Ren, J.; Wan, X.; Zhou, L. Comparative study of cloud liquid water and rain liquid water obtained from microwave radiometer and micro rain radar observations over central China during the monsoon. *J. Geophys. Res. Atmos.* **2020**, *125*, e2020JD032456. [CrossRef]
25. Zheng, Z.; Xu, G.; Li, Q.; Chen, C.; Li, J. Effect of precipitation on reducing atmospheric pollutant over Beijing. *Atmos. Pollut. Res.* **2019**, *10*, 1443–1453. [CrossRef]
26. Haurwitz, M.; Brier, G. A Critique of the Superposed Epoch Analysis Method: Its Application to Solar–Weather Relations. *Mon. Weather. Rev.* **1981**, *109*, 2074–2079. [CrossRef]